*American Mineralogist, Volume 89, pages 1533–1539, 2004*

# Synthesis of REE and Y phosphates by Pb-free flux methods and their utilization as standards for electron microprobe analysis and in design of monazite chemical U-Th-Pb dating protocol

**D.J. CHERNIAK,[1,*] J. PYLE,[1] AND JOHN RAKOVAN[2]**

[1]Department of Earth and Environmental Sciences, Rensselaer Polytechnic Institute, Troy, New York 12180, U.S.A.
[2]Department of Geology, Miami University, Oxford, Ohio 45056, U.S.A.

## ABSTRACT

(REE,Y) phosphates were synthesized in a 1 atm furnace by flux-growth methods involving Pb-free fluxes. Microcrystalline (REE,Y) phosphate was precipitated from a solution of (REE,Y) chlorides or nitrates plus ammonium dihydrogen phosphate, and mixed with a $M_2CO_3$ (M = Li or Na)-$MoO_3$ flux (75:25:2 molar ratio $M_2CO_3$:$MoO_3$:$REEPO_4$). Crystal growth was achieved over the temperature range 1350–870 °C, with extended (15 h) high-*T* soaking, and cooling rates of 3 °C/h. Crystals grown by this method are clear, generally inclusion-free, up to several mm in length, and are easily extracted from the water-soluble flux. Crystal size and habit are influenced by the alkali component of the flux. Successful LREE phosphate synthesis is favored by both Li-and Na-bearing fluxes, whereas better results for Y and MREE-HREE phosphates were achieved with Na-bearing fluxes. Li-bearing fluxes produced LREE phosphates with an overall platy habit, in contrast to more prismatic-to-equant LREE-MREE phosphates produced with Na-bearing fluxes.

Structural refinements of single-crystal X-ray diffraction data show that $LREEPO_4$ (La-Gd) crystallize with the monoclinic monazite structure, and $HREEPO_4$ (Tb-Lu) plus $YPO_4$ crystallize with the tetragonal xenotime structure. Element distribution maps of synthetic $REEPO_4$ reveal homogeneous distribution of REE and P at grain-size scale and below, and both wavelength-dispersive (WD) spectral scans and quantitative electron microprobe analyses show no other elements (e.g., flux inclusions) present at significant levels.

The synthetic phosphates grown with this method are suitable for use as electron microprobe standards and as compositionally simplified monazite analogs for use in the design of U-Th-Pb chemical dating protocols. WD scans of synthetic unary and ternary (La-Ce-Nd) phosphates reveal that Ar X-ray detectors produce non-filterable LREE escape peaks with pulse-height analyzers optimized for Pb analysis. Such LREE escape peaks complicate collection of both U and Pb peak and background counts. Due to the larger energy difference between LREE peaks and Xe (relative to Ar), LREE escape peaks produced in Xe detectors are filterable with pulse height analyzers, resulting in LREE-free spectra over the wavelength range sampled for Pb peak and background collection.

## INTRODUCTION

REE phosphates have traditionally and successfully been grown with Pb-bearing fluxes (e.g., Feigelson 1964; Smith and Wanklyn 1974; Wanklyn 1977, 1978; Rappaz et al. 1980, 1981). However, growing REE phosphates via these methods can pose some difficulty when the intention is to use the synthetic crystals for standards for U-Th-Pb electron microprobe dating of monazites, or in diffusion experiments exploring diffusion of Pb or other heavy elements, since the phosphates that are produced tend to contain inclusions of the Pb-bearing flux or to incorporate Pb structurally into the mineral lattice. Other techniques, including hydrothermal synthesis (e.g., Montel 1989; Anthony 1957) and flux growth using $KH_2PO_4$ (e.g., Anthony 1965), $K_2Mo_3O_{10}$ (Nekrasov and Novikov 1991), and $Na_4P_2O_7$ (e.g., Samatov et al. 1982) fluxes, yield predominantly small crystals or inconsistent results. A method adapted from techniques used for synthesizing zircon has been developed for growing REE and Y phosphates of good crystal quality and appreciable size (up to several mm). This technique employs molybdenum oxide-alkali carbonate fluxes. Zircon growth via a lithium molybdate flux was pioneered by Espig (1960) and further refined by other researchers (e.g., Chase and Osmer 1966; Ball and Wanklyn 1976); Ballman and Laudise (1965) reported successful zircon growth with both $Li_2O{\cdot}3MoO_3$ and $Na_2O{\cdot}3MoO_3$ fluxes. The flux composition used in the present study most closely approximates the materials and proportions used in the work of Suzuki et al. (1992).

In this paper, we describe the synthesis method and present analyses of crystal composition and structure of the synthesized REE phosphates. We also consider the influence of flux composition on crystal growth and habit across the series of rare earth phosphates from light to heavy REE. Since the Pb-free rare-earth phosphates have considerable potential for use in design of monazite U-Th-Pb chemical dating protocols, we present results of electron microprobe analyses of unary and ternary LREE phosphates, using both Xe and Ar detectors, which highlight the

* E-mail: chernd@rpi.edu

value as standards of the LREE phosphates grown by this method, as well as the utility of Xe detectors for these analyses.

## CRYSTAL SYNTHESIS

Crystals were grown with a flux consisting of $MoO_3$ and either $Li_2CO_3$ or $Na_2CO_3$. The flux components were mixed in a (molar) ratio of 75:25 $MoO_3$:$Li_2CO_3$ or $Na_2CO_3$. Rare earth (or Y) phosphate was mixed with the flux in a (molar) ratio of 100:2 flux:$REEPO_4$. The REE and Y phosphates were added in powder form, either purchased as reagents or synthesized. Phosphate powders were synthesized (in an adaptation of the method of Abraham et al. 1980, and similar to the approach taken by Montel et al. 2002) by dissolving REE nitrates in distilled water, heating the solution in a Pyrex beaker on a hotplate to boiling, and adding ammonium dihydrogen phosphate. A microcrystalline REE phosphate precipitate was then formed. This material was placed overnight in a drying oven to evaporate water and other volatiles; it was then heated for an hour at 500 °C, and for an additional hour in an alumina or porcelain crucible at 800 °C.

The flux and REE phosphate powders were thoroughly mixed, then placed in a covered platinum crucible. Crucibles were heated to 1350 ºC (for $Li_2CO_3$:$MoO_3$ flux) or 1280 ºC (for $Na_2CO_3$:$MoO_3$ flux) in air in a Deltech tube furnace (with a 1.5" i.d. mullite furnace tube) with $MoSi_2$ heating elements, "soaked" for 15 h at this temperature, then cooled at 3 ºC/h to 870 °C. The crucible was then removed from the furnace. After cooling, crystals were freed from the residual flux by ultrasonic cleaning in baths of distilled water. The crystals produced were clear, mostly free of inclusions, of good crystal form, and up to several mm in length.

Phosphates of each of the REE (plus Y) were synthesized separately. In addition, a mixed LREE phosphate was grown, of nominal composition 25 mol% La, 55 mol% Ce, and 20 mol% Nd. This molar ratio approximates a La-Ce-Nd ratio typical of metamorphic monazite (Pyle et al. 2001). The mixed LREE phosphate was grown with the $Na_2CO_3$:$MoO_3$ flux as outlined above. Two different synthesis experiments were performed. One added a mixture of the pre-synthesized Nd, Ce, and La phosphate powders (prepared as above) in appropriate proportions (i.e., 25 mol% $LaPO_4$, 55 mol% $CePO_4$, and 20 mol% $NdPO_4$) to the flux material. The other experiment started with a mixed LREE phosphate, made by dissolving Nd, Ce, and La nitrates (in 20:55:25 molar proportions) together in water, heating, and adding ammonium dihydrogen phosphate to precipitate a mixed LREE phosphate powder. The powder was then treated, as described above, for the single REE phosphate powders, and mixed with the flux. In both cases of mixed LREE phosphate syntheses, the flux to phosphate molar ratio was 100:2, and ramp and soak cycles were the same as for syntheses of unary REE phosphates using the $Na_2CO_3$:$MoO_3$ flux.

## RESULTS

A summary of the syntheses is presented in Table 1. Photographs of the products are shown in Figures 1 and 2. We found that the $Li_2CO_3$:$MoO_3$ flux worked best for synthesis of the LREE phosphates. The middle to heavy rare earth phosphates (as well as $YPO_4$) grown with this flux were of lesser quality; for example, $YPO_4$ and $YbPO_4$ crystals were not well formed and had a "frosted" appearance, and Dy and Tb phosphate syntheses produced small yields of small crystals. Better results were achieved for $YPO_4$ and middle to heavy REE phosphates by replacing the $Li_2CO_3$ with an equivalent molar amount of $Na_2CO_3$. The $Na_2CO_3$:$MoO_3$ flux also worked quite well for some of the lighter REE; for example, good-quality, large crystals of $PrPO_4$ and $NdPO_4$ were grown with this system. However, for the heaviest rare earths (Yb and Lu), grain size for crystals grown in the $Na_2CO_3$:$MoO_3$ flux dropped considerably (most notably for Lu), as did crystal yield. Synthesis experiments were also tried for the heavy rare earth Yb using a $K_2CO_3$:$MoO_3$ flux (with the same molar ratios as Na and Li carbonate fluxes), but only microcrystalline material was obtained.

In successful syntheses using both the $Na_2CO_3$:$MoO_3$ and $Li_2CO_3$:$MoO_3$ fluxes, crystal growth was concentrated toward the bottom of the crucible. It should also be noted that the col-

**TABLE 1.** Summary of results of flux synthesis of REE and Y phosphates

| Phosphate | Flux | Habit | Color |
|---|---|---|---|
| $LaPO_4$ | $Li_2CO_3$:$MoO_3$ | monoclinic-La habit, platy | pale green |
| $CePO_4$ | $Li_2CO_3$:$MoO_3$ | monoclinic-La habit, platy | pale green |
| $CePO_4$ | $Na_2CO_3$:$MoO_3$ | monoclinic, blocky | pale green |
| $PrPO_4$ | $Li_2CO_3$:$MoO_3$ | monoclinic-La habit, platy | bright green |
| $PrPO_4$ | $Na_2CO_3$:$MoO_3$ | monoclinic, blocky | bright green |
| $NdPO_4$ | $Li_2CO_3$:$MoO_3$ | monoclinic-La habit, platy | purple |
| $NdPO_4$ | $Na_2CO_3$:$MoO_3$ | monoclinic, blocky | purple |
| $SmPO_4$ | $Li_2CO_3$:$MoO_3$ | monoclinic-La habit, platy | yellow |
| $SmPO_4$ | $Na_2CO_3$:$MoO_3$ | monoclinic, blocky | yellow |
| $EuPO_4$ | $Li_2CO_3$:$MoO_3$ | monoclinic, platy | colorless |
| $EuPO_4$ | $Na_2CO_3$:$MoO_3$ | monoclinic-prismatic | colorless |
| $GdPO_4$ | $Li_2CO_3$:$MoO_3$ | monoclinic, platy | blue-green |
| $GdPO_4$ | $Na_2CO_3$:$MoO_3$ | monoclinic-prismatic | blue-green |
| $TbPO_4$ | $Li_2CO_3$:$MoO_3$ | tetragonal, small crystals | brown/green |
| $TbPO_4$ | $Na_2CO_3$:$MoO_3$ | tetragonal | brown/green |
| $DyPO_4$ | $Li_2CO_3$:$MoO_3$ | tetragonal, small crystals | pale brown |
| $DyPO_4$ | $Na_2CO_3$:$MoO_3$ | tetragonal | brown |
| $HoPO_4$ | $Na_2CO_3$:$MoO_3$ | tetragonal | dark red |
| $ErPO_4$ | $Na_2CO_3$:$MoO_3$ | tetragonal | dark red |
| $TmPO_4$ | $Na_2CO_3$:$MoO_3$ | tetragonal | yellow/brown |
| $YbPO_4$ | $Li_2CO_3$:$MoO_3$ | tetragonal, pitted faces | yellow/green |
| $YbPO_4$ | $Na_2CO_3$:$MoO_3$ | tetragonal | yellow/green |
| $LuPO_4$ | $Na_2CO_3$:$MoO_3$ | tetragonal | yellow/green |
| $YPO_4$ | $Li_2CO_3$:$MoO_3$ | tetragonal, pitted faces | pale brown |
| $YPO_4$ | $Na_2CO_3$:$MoO_3$ | tetragonal | pale brown |

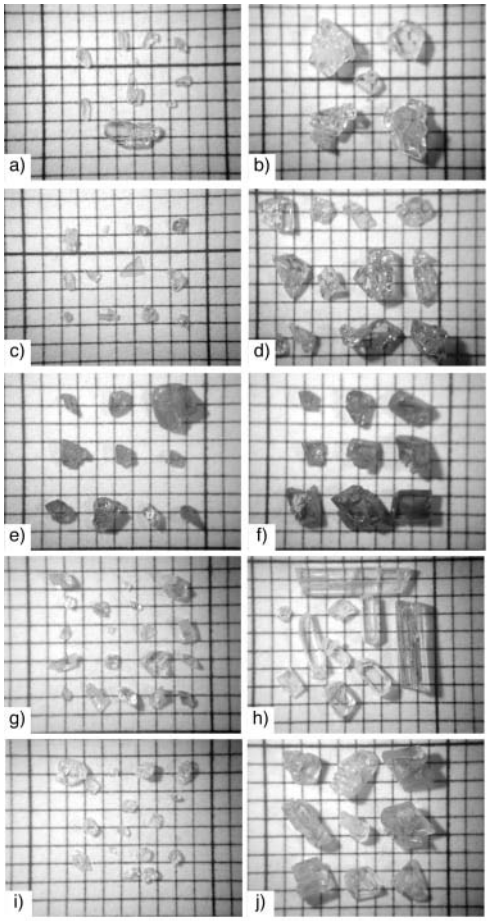


**FIGURE 1.** Photographs of experimental products produced with both $Li_2CO_3$-$MoO_3$ flux and $Na_2CO_3$-$MoO_3$ flux. The crystals in the left column (**a**, **c**, **e**, **g**, **i**) were produced with an $Li_2CO_3$-$MoO_3$ flux, and the crystals in the right column were produced with an $Na_2CO_3$-$MoO_3$ flux. (**a**, **b**) $CePO_4$, (**c**, **d**) $PrPO_4$, (**e**, **f**) $NdPO_4$, (**g**, **h**) $EuPO_4$, (**i**, **j**) $GdPO_4$. Grid unit = 1 mm.

ors of synthesized crystals were consistent with those of the precursor powders, and crystals of a given REE grown in both $Na_2CO_3$:$MoO_3$ and $Li_2CO_3$:$MoO_3$ fluxes were the same color, indicating that components in the flux that may be introduced into crystals as impurities are unlikely to be the source of crystal coloration. Further, Ce phosphates grown by hydrothermal methods (Cherniak et al. 2004) and Nd and Sm phosphates in the author's possession (obtained from L. Boatner) grown with Pb pyrophosphate fluxes (e.g., Rappaz et al. 1980) have the same colors as those grown with the $Na_2CO_3$:$MoO_3$ and $Li_2CO_3$:$MoO_3$ flux methods, despite the differences in growth environments and the presence of different potential crystal impurities in each of these environments.

Compositions and structures of the synthesized crystals were investigated with electron microprobe analysis and X-ray diffraction.

## XRD

Phases were identified from refined unit-cell parameters determined from single crystal X-ray diffraction data. Crystal fragments were mounted on a Bruker Apex CCD diffractometer, which used graphite-monochromated Mo$K\alpha$ radiation. A small area of reciprocal space over a large angular range was sampled and between 11 and 89 reflections were extracted to determine symmetry and to refine unit-cell parameters (Table 2) using the Bruker SMART program (Bruker AXS Inc. 2001). Unit-cell parameters were used to search the National Institute of Standards Inorganic Crystal Structure Database for phase identification.

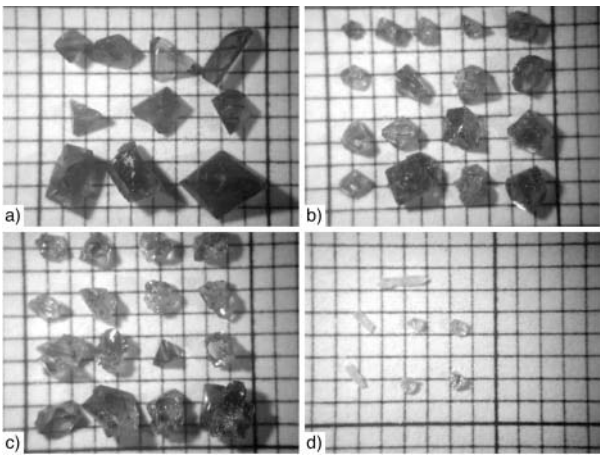


**FIGURE 2.** Photographs of experimental products produced with the $Na_2CO_3$-$MoO_3$ flux alone. (**a**) $HoPO_4$, (**b**) $ErPO_4$, (**c**) $TmPO_4$, (**d**) $LuPO_4$. Grid unit = 1 mm.

## Electron microprobe analyses

Several qualitative and quantitative tests were done to confirm the mineralogical identity of the experimental products, as well as the degree of intracrystalline homogeneity. All analyses were performed with a JEOL 733 Superprobe EMP at Rensselaer Polytechnic Institute, equipped with five wavelength dispersive spectrometers, TAP, PET, LDE1, and LiF diffraction crystals, and both gas flow P10 (90% Ar, 10% $CH_4$) and sealed Xe detectors; the complete EMP configuration is given in Pyle et al. (2004). All crystals examined by microprobe were mounted in epoxy, polished to a 1 μm diamond-paste level, then finished with 1–2 hours of chemical-mechanical polishing using a colloidal silica suspension with an average particle size of 0.05–0.25 μm.

First, element distribution maps were generated to check for the presence of moderate to large flux inclusions in the crystal faces. Phosphates of La, Ce, and Nd were mapped for REE and P distribution. P and the mapped REE are distributed homogeneously across the crystal surface. Pits in the crystal surface may mark the former location of inclusions of $Li_2MoO_4$ (see below).

After reconnaissance mapping, detailed wavelength scans were performed on several unary REE phosphates (La, Ce, Nd, Sm, Gd, Dy, Er, Yb), plus $YPO_4$, and a ternary La-Ce-Nd phosphate. The following six unary REE phosphate scans are shown in Figure 3: $LaPO_4$ (Fig. 3a), $CePO_4$ (Fig. 3b), $NdPO_4$ (Fig 3c), $GdPO_4$ (Fig. 3d), $DyPO_4$ (Fig. 3e), and $ErPO_4$ (Fig. 3f). Scanning over the range 200–100 mm on a LiF diffraction crystal (2.871–1.436 Å) coupled with a Xe detector produced only the characteristic X-ray lines of the REE present (Figs. 3a–f). Similarly, scans of Sm, Yb, and Y phosphate showed only characteristic X-ray lines of the REE (or Y) present over the crystal range scanned for Figure 3 [$YPO_4$ was scanned for characteristic X-ray lines over the range 240–190 mm (7.49–5.93 Å) on PET].

An identical set of scans was performed on a ternary (La,Ce,Nd) phosphate (Fig. 4). The scans of the mixed-powder ternary REE phosphate and the single powder ternary REE phosphate are virtually identical (Figs. 4a and 4b). All of the major characteristic X-ray peaks of La, Ce, and Nd were present. The lowest intensity (I ~ 1%) peaks clearly identified are the $L\gamma_4$ peaks of La, Ce, and Nd.

Both the mixed-powder and single-powder (La, Ce, Nd) phosphates were analyzed. The analytical protocol is described in Pyle (2001). The REE phosphates synthesized for this study were used as microprobe standards, and the following elements were measured: P, Si, Ca, Pb, Th, U, Y, La, Ce, Pr, Nd, Sm, Gd, Tb, Dy, and Er. A core and rim analysis of both phases was

**TABLE 2.** Refined unit-cell parameters and phase identification of synthesized REE-phosphate compounds

| Composition<br>Symmetry | $YPO_4$<br>tetragonal | $PrPO_4$(Li)<br>monoclinic | $YbPO_4$(Na)<br>tetragonal | $PrPO_4$(Na)<br>monoclinic | $LaPO_4$<br>monoclinic | $GdPO_4$<br>monoclinic |
|---|---|---|---|---|---|---|
| *a* (Å) | 6.8869(149) | 6.4319(7) | 6.7971(0.1172) | 6.4304(15) | 6.5089(12) | 6.3415(13) |
| *b* (Å) | 6.8828(85) | 6.9527(17) | 6.8158(0.0734) | 6.9929(16) | 7.0790(13) | 6.8542(11) |
| *c* (Å) | 6.0172(85) | 6.7432(16) | 5.9659(0.095) | 6.7683(14) | 6.8432(14) | 6.6543(15) |
| α (°) | 89.954(87) | 90.030(19) | 90.014(0.267) | 90.061(011) | 90.090(02) | 90.022(13) |
| β (°) | 89.875(124) | 103.665(21) | 90.080(0.599) | 103.417(014) | 103.241(013) | 104.016(14) |
| γ (°) | 89.965(87) | 90.001(16) | 90.007(0.29 5) | 90.032(016) | 89.962(016) | 90.021(01) |
| No. of Ref.* | 11 | 65 | 24 | 81 | 80 | 89 |
| Phase | xenotime | monazite | xenotime | monazite | monazite | monazite |

* The number of reflections used in the least squares refinement of unit-cell parameters.

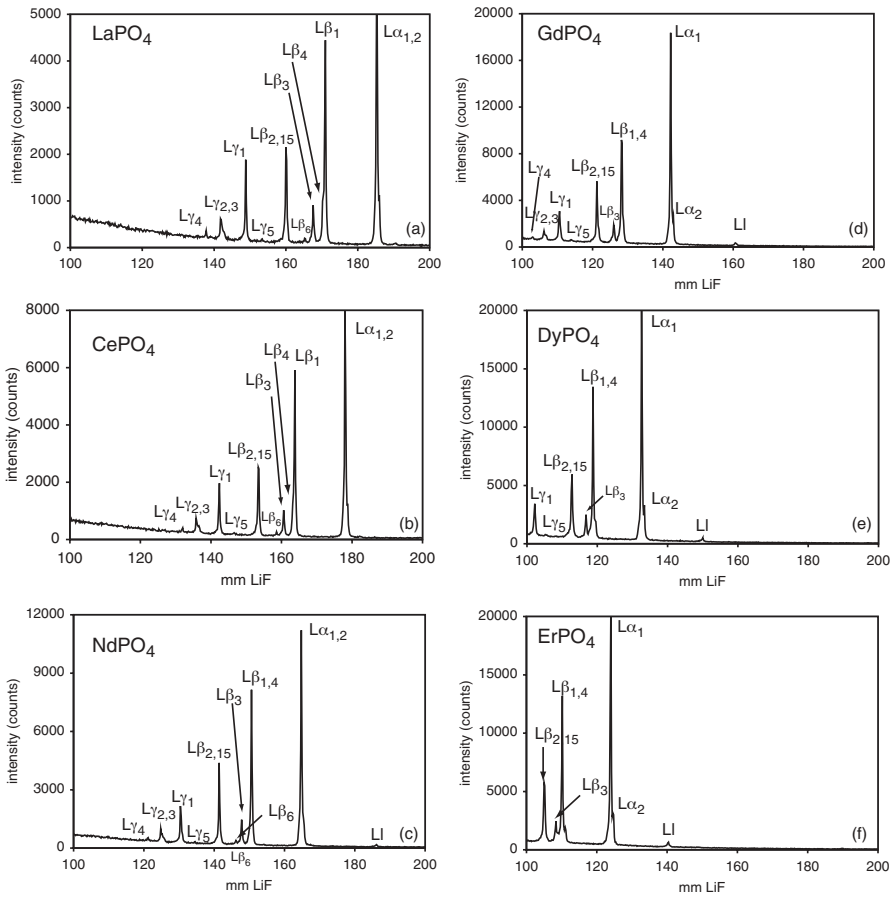


**FIGURE 3.** Wavelength dispersive scans of single-crystal synthesis products. (**a**) $LaPO_4$, (**b**) $CePO_4$, (**c**) $NdPO_4$, (**d**) $GdPO_4$, (**e**) $DyPO_4$, (**f**) $ErPO_4$. Scans were performed with an LiF diffraction crystal and Xe detector, with 140 mm Rowland Circle and open (3 mm) X-ray collimators. The scan interval was 200–100 mm (2.871–1.436 Å) for all samples shown. The peaks are labeled according to Siegbahn notation. The scan conditions included 15 kV accelerating voltage, 75 nA cup current, 0.2 mm step size, and 5 second dwell time per step. All peaks shown are first-order lines.

performed; the results are listed in Table 3. All elements other than La, Ce, Nd, and P were not detectable at the detection limits shown in Table 3. All elements below the detection limits were set to zero concentration, resulting in analytical totals between 98.5 and 98.9 wt% oxide, with calculated cation totals of 1.989 to 1.996 per 4 O atoms.

The single-powder REE phosphate showed no discernible compositional difference between the core and rim and gives an average composition ($2\sigma$) of $La_{0.2881(2)}Ce_{0.5212(24)}Nd_{0.1908(26)}PO_4$. The mixed powder REE phosphate likewise showed no discernible core-rim compositional difference and gives an average composition of $La_{0.2718(4)}Ce_{0.5286(7)}Nd_{0.1996(13)}PO_4$. The results compare quite favorably (within 3%) to the target composition of $(La_{0.25}Ce_{0.55}Nd_{0.20})PO_4$.

**TABLE 3.** Electron microprobe analyses (wt% oxide) of ternary (La, Ce, Nd) phosphate

| Sample analysis | LCNP- h core | LCNP- h rim | LCNP-m core | LCNP-m rim | d.l. (wt% oxide) |
|---|---|---|---|---|---|
| $P_2O_5$ | 30.63 | 30.11 | 30.07 | 30.33 | 0.720 |
| $SiO_2$ | bdl | bdl | bdl | bdl | 0.009 |
| CaO | bdl | bdl | bdl | bdl | 0.008 |
| PbO | bdl | bdl | bdl | bdl | 0.114 |
| $ThO_2$ | bdl | bdl | bdl | bdl | 0.132 |
| $UO_2$ | bdl | bdl | bdl | bdl | 0.094 |
| $Y_2O_3$ | bdl | bdl | bdl | bdl | 0.081 |
| $La_2O_3$ | 19.36 | 19.59 | 18.37 | 18.47 | 0.168 |
| $Ce_2O_3$ | 35.24 | 35.74 | 36.00 | 36.18 | 0.149 |
| $Pr_2O_3$ | bdl | bdl | bdl | bdl | 0.141 |
| $Nd_2O_3$ | 13.31 | 13.32 | 14.01 | 13.93 | 0.173 |
| $Sm_2O_3$ | bdl | bdl | bdl | bdl | 0.094 |
| $Gd_2O_3$ | bdl | bdl | bdl | bdl | 0.155 |
| $Tb_2O_3$ | bdl | bdl | bdl | bdl | 0.144 |
| $Dy_2O_3$ | bdl | bdl | bdl | bdl | 0.058 |
| $Er_2O_3$ | bdl | bdl | bdl | bdl | 0.053 |
| total | 98.54 | 98.76 | 98.45 | 98.91 | |
| $X_{LaPO4}$ | 0.2880 | 0.2882 | 0.2715 | 0.2721 | |
| $X_{CePO4}$ | 0.5203 | 0.5220 | 0.5281 | 0.5291 | |
| $X_{NdPO4}$ | 0.1917 | 0.1898 | 0.2005 | 0.1987 | |

*Notes:* LCNP-h = La-Ce-Nd phosphate prepared as a single homogeneous precipitate; LCNP-m = La-Ce-Nd phosphate prepared as a mixture of separately precipitated unary La, Ce, and Nd phosphates.
Theoretical composition 0.25-0.55-0.20 ($X_{LaPO4}$-$X_{CePO4}$-$X_{NdPO4}$).
Detection limits at 25 kV, 50 nA for analysis times given in Pyle (2001).

## DISCUSSION

### Crystal growth and habit

Bondar et al. (1976; as cited in Boatner and Sales 1988) reported on observed structural types for lanthanide orthophosphates. From La to Eu, the high-temperature form is monoclinic. For Gd to Lu (and Y), it is tetragonal. The REE phosphates from Gd to Dy, which are tetragonal in the high-temperature form, can also have an intermediate monoclinic form. In addition, the phosphates from La to Dy have a low-temperature hexagonal form, which makes the transition to monoclinic structure at temperatures between 400 and 600 °C.

It might be argued that a "critical cutoff," i.e., where the $Na_2CO_3$:$MoO_3$ flux works better (in producing higher-quality crystals) than the $Li_2CO_3$:$MoO_3$ flux, would occur around Gd, since the high-temperature form for REE phosphates for Gd and

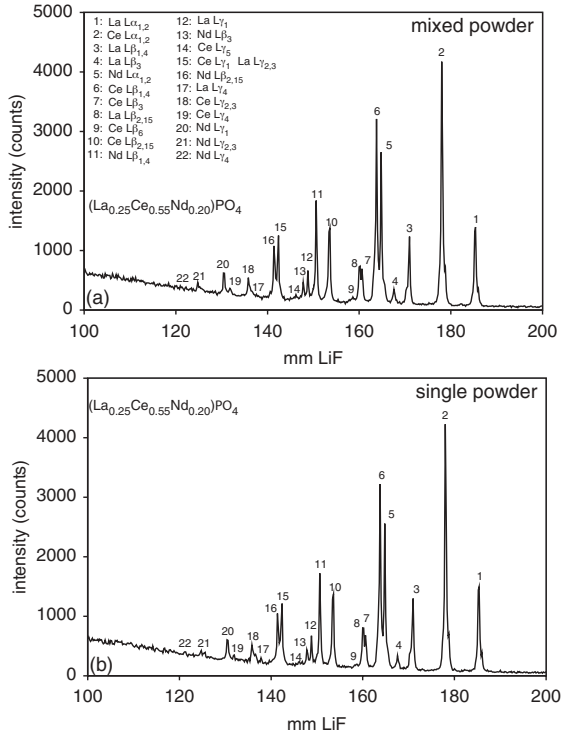


**FIGURE 4.** Wavelength dispersive scans of single-crystal ternary (La-Ce-Nd) rare earth phosphate. Scan (**a**) was obtained from a single crystal prepared by mixing microcrystalline $LaPO_4$, $CePO_4$, and $NdPO_4$ powders in the desired (25-55-20) molar proportion. Scan (**b**) was obtained from a single crystal prepared with a homogeneous REE phosphate precipitate of the desired composition. Probe analyses and measured mole fractions of crystals scanned in (**a**) and (**b**) are listed in Table 3. EMP setup and scan conditions are identical to those given in Figure 4. Characteristic X-ray peak numbers are keyed to the list in (**a**). All peaks shown are first-order lines.

heavier REEs (as well as Y) is tetragonal, whereas that for the lighter REEs is monoclinic. However, Wanklyn (1978) found that, in the growth of REE phosphates with Pb pyrophosphate flux with $PbF_2$, Gd phosphates were monoclinic whereas Dy and Tm were tetragonal; we observed similar differences in crystal morphology for crystals grown in the $Na_2CO_3$:$MoO_3$ flux.

It should be stressed, however, that the structural differences between the monoclinic and tetragonal forms are small, and some of our other findings do suggest a lack of a simple correlation between flux utility and crystal structure. Crystals of Ce, Sm, Nd, Pr, and Eu phosphates grown with the $Na_2CO_3$:$MoO_3$ flux are fairly large and of good quality. Interestingly, while high-quality crystals of these LREE phosphates are grown with both $Na_2CO_3$:$MoO_3$ and $Li_2CO_3$:$MoO_3$ fluxes, their crystal habits differ, with those from the Na flux possessing a prismatic morphology (e.g., Boatner and Sales 1988) and those grown in the Li flux having a more platy habit. Yields and crystal size tend to be somewhat greater for the LREE crystals grown with the $Na_2CO_3$:$MoO_3$ flux. Differences in crystal habit have been noted in other studies using flux growth methods. Wanklyn (1983) was able to "tailor" flux compositions to produce rare-earth phosphate crystals of desired habit by changing the acid-base ratio in the system $Dy_2O_3$-PbO-$P_2O_5$. She found that growth rates were influenced by the types of complex ions present in the flux, with these in turn determined by the availability of O atoms, supplied by PbO in this system. With more O atoms, there was a tendency to form the smaller $(PO_4)^{3-}$ complexes, which would diffuse more easily and facilitate crystal growth. Fewer, larger, and more equidimensional crystals were obtained from melts with higher basic oxide concentrations.Ehrenhaut and Pollnau (2002) have found differences in crystal habit of $BaSO_4$ crystals grown in alkali chloride fluxes. Those grown in a LiCl-KCl flux had larger aspect ratios, while crystals grown in a CsCl-KCl-NaCl flux were shorter with a compact prismatic habit. The presence of different alkalis in fluxes can also influence crystal size, shown by Fujii et al. (1992) in their study of $PbTiO_3$ crystal growth. Crystals grown in a PbO flux with the addition of Na or Li carbonates were larger than crystals grown with PbO alone, and the crystals grown in the flux containing Na were larger than those grown with Li in the system.

It seems likely that in the flux systems reported here the presence and proportions of various ionic species in the melt and their chemical interactions with the various lanthanides, will, as in the case of the Pb-based flux systems described by Wanklyn (1983) and Wanklyn et al. (1983), influence the size, aspect ratio, habit, and quality of the crystals. In the systems we describe, in analogy with the work of Wanklyn (1983), the basic oxides are $Na_2O$ and $Li_2O$, and the acidic oxide is $MoO_3$, which are present in a 1:3 molar ratio. When basic oxides are present in relatively high concentrations, smaller complexes form, but when there is less basic oxide, large highly charged anions may form which can impede the crystal growth process, thus affecting growth rates and crystal habit. The types of complexes formed may vary with the different alkali elements present, as well as among the series of lanthanides, given their differences in ionic radius. While beyond the scope of this paper, further investigation to better characterize these influences is clearly warranted.

### Use of compositionally simple "monazite" in design of U-Th-Pb chemical dating protocol

The recent proliferation of electron microprobe monazite dating has spurred studies addressing the issue of the compositional complexity of natural monazite as it relates to analytical problems associated with the monazite chemical dating technique (Pyle et al. 2004; Jercinovic and Williams 2004). The production of unary rare-earth phosphates as microprobe standards is a great aid in both addressing the complexities of chemical dating of monazite and design of chemical dating analysis protocols. With Pb-free unary, binary, or ternary REE phosphates, the difficulties of designing a workable monazite chemical dating protocol can be addressed one, two, or three elements at a time, instead of 10–15 elements at a time, as must be the case for natural REE- and actinide-bearing monazites.

An example of such a difficulty in monazite chemical dating protocols involves the use of different detector gases. The problems involved with selection of Xe vs. Ar as a detector gas are clearly highlighted by examination of unary and ternary REE phosphates. The issue of detector gas and its relationship to production of escape peaks of second-order REE lines is briefly summarized here.

In chemical dating of monazite, maximization of lead analyti-

cal precision is the single most important aspect of the analytical protocol. As a result, detector settings for lead analysis include narrow voltage windows, so as to filter unwanted, higher-order X-ray lines, thus producing a "cleaner" wavelength-dispersive spectrum. However, energy differences between second-order lines of abundant LREE (La, Ce, Nd) and the critical excitation energy of the Ar*K* shell result in voltage pulses nearly identical in energy to the lead voltage pulse, so that overlapping of the Pb voltage pulse by the second-order LREE voltage pulse occurs. These voltage pulses cannot be filtered without also filtering significant portions of the lead signal, and thus are passed to the X-ray counter. However, the energy difference between the second-order lines of the abundant LREE and the critical excitation energy of the Xe$L_{III}$ shell result in LREE second order escape peaks that have voltage pulse energies dissimilar to the lead voltage pulse energy. As a result, no overlap of Pb and second-order LREE voltage pulses occurs in Xe detectors, with the result that unwanted LREE signal can be filtered with a narrow voltage window.

Scans of unary and ternary REE phosphates, using both Ar and Xe detectors, are shown in Figure 5. Ar detector scans are shown as grey lines, and Xe detector scans are shown as black lines. Scans were done with a PET diffraction crystal over the range 200–100 mm (6.243–3.121 Å), with scan conditions of 15 kV, 75 nA cup current, 0.2 mm step size, and 5 s/step dwell time.

The wavelength range cited above is crucial to chemical dating of monazite, as the wavelengths of the *M*α and *M*β lines of Pb, Th, and U all fall in this range, as well as background collection positions for these lines. Despite the narrow voltage windows used for on all four detectors (detector settings for all four spectrometers are identical to those used for lead analysis), the Ar-REE energy differential results in voltage pulses that are passed to the X-ray counter, and a spectrum containing high-intensity second-order lines of La (Fig. 6a), Ce (Fig. 6b), and Nd (Fig. 6c) is produced. The larger Xe-REE energy differential results in filterable voltage pulses; these pulses are not passed to the X-ray counter, resulting in a spectrum free of the second-order LREE lines (Figs. 5a–c).

As the energy of the REE line increases, the Ar-REE energy differential also increases, so that for energies greater than that of Nd (Fig. 5c), voltage pulses of the REE are effectively filtered with Ar detectors using narrow voltage windows. This is apparent in the scans of $DyPO_4$ and $ErPO_4$, where an insignificant proportion of the energy in the Ar detector is passed to the counter, resulting in MREE-HREE *L*α peaks (Figs. 5d and 5e) that are approximately 10% of the magnitude of the LREE *L*α peaks. With narrow-window configurations, Xe detectors will generate non-filterable energies for some second-order and third-order lines of the MREE and HREE (Figs. 5c–e), but the intensities of

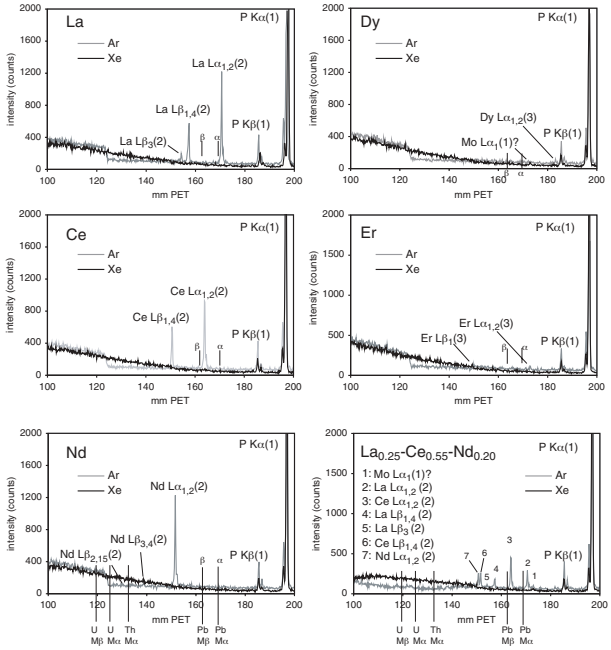


**FIGURE 5.** Wavelength-dispersive scans of single crystal synthesis products. (**a**) $LaPO_4$, (**b**) $CePO_4$, (**c**) $NdPO_4$, (**d**) $DyPO_4$, (**e**) $ErPO_4$, (**f**) $(La_{0.25}Ce_{0.55}Nd_{0.20})PO_4$. The scans were performed with a PET diffraction crystal and both Ar (gray line) and Xe detectors (black line), with 140 mm Rowland circle and open (3 mm) X-ray collimators. The scan interval was 200–100 mm (6.243–3.121 Å). The scan conditions were identical to those given in Figure 4. The numbers in parentheses next to Siegbahn notation indicate the order of the X-ray peak. Approximate positions of the Pb*M*α and *M*β peaks are indicated by vertical lines labeled "α" and "β", respectively. The positions of Pb*M*α, Pb*M*β, Th*M*α, U*M*α, and U*M*β are labeled on Figures 5e and 5f.

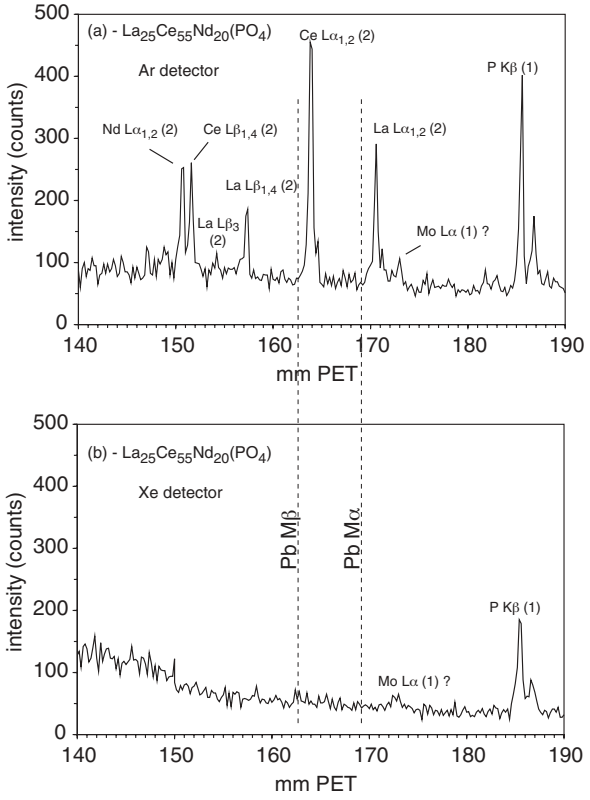


**FIGURE 6.** Enlargement of Figure 5f, showing a portion of the WD scan of $(La_{0.25}Ce_{0.55}Nd_{0.20})PO_4$, from 190–140 mm PET, for (**a**) the Ar detector and (**b**) the Xe detector. Approximate positions of the Pb*M*α and *M*β peaks are indicated by vertical lines labeled "Pb*M*α" and "Pb*M*β", respectively.

the energies passed to the detector are trivial (~10% of Ar escape peak intensities), owing to greater absorption of Xe X-rays in Xe gas (Scott et al. 1995).

In natural monazites, as approximated by the ternary La-Ce-Nd phosphate (Figs. 5f and 6), Ar detectors produce a much more complex WD spectrum than do Xe detectors. Analysis of either Pb$M\alpha$ or Pb$M\beta$ is complicated by potential interferences with the second-order La, Ce, and Nd peaks passed by the detector. Even if sufficient wavelength resolution exists (e.g., for a 160 mm Rowland circle) to separate lead and REE peaks, interference-free background collection is still problematic. In a natural monazite, second-order lines of Pr, Sm, Th, and U would occur in the Ar-detector spectrum, in addition to first-order lines of Th, U, Y, and possibly S, that would occur in both Ar- and Xe-detector spectra, greatly increasing the complexity of the WD spectrum. These observations are borne out in Figure 6. The positions of the Pb$M\alpha$ and $M\beta$ peaks are near to the lower shoulders of the La$L\alpha$ (2) and Ce$L\alpha$ (2) peaks, respectively. Additionally, the Ar$K$ absorption edge, which may pose a problem for U analysis on Ar detectors, does not appear in scans using Xe detectors (Figs. 5a–e).

As an aside, if Mo is present as an inclusion in monazite, it would be detected in a wavelength scan over this range. An Mo$L\alpha$ peak (first-order) may be present in the scan of $DyPO_4$ (Fig. 5d), as well as in $LaPO_4$ (Fig. 5a) and the ternary REE phosphate (Figs. 5f and 6). The Mo peak, if present, is more clearly discernible with a Xe scan, as it is not masked by the shoulder of the second-order La$L\alpha$ peak. Peak 1 in Figure 5f is at approximately the same position as the second-order $NdL_l$ peak, but as this peak does not appear in the scan of $NdPO_4$ (Fig. 5c), and peak number 1 is present on both Ar- and Xe-detector spectra (Figs. 5f and 6), it is more likely to be the first-order Mo$L\alpha$ peak, which is passed by both detectors. If Mo is present, it is likely in the form of minute inclusions of $Li_2MoO_4$, rather than disseminated Mo, which would likely not be detectible by WD scanning. Inclusions of $Li_2MoO_4$ may be responsible for linear growth features observed in these crystals (R. Uhrin, pers comm., 2004), and may be have been formerly present in pits in the surfaces of several synthetic crystals grown in this study. In any case, the Mo is present in small quantities, and should not hinder accurate Pb analysis.

## ACKNOWLEDGMENTS

The authors thank B. Watson for advice on and discussions concerning general synthesis of accessory minerals, and D. Wark and K. Becker for maintenance of the JEOL 733 Superprobe EMPA housed at Rensselaer Polytechnic Institute. An earlier version of this manuscript benefited from constructive reviews by J.-M. Montel and R. Uhrin, and the editorial handling of J. Ayers. This work was supported in part by NSF grants EAR-0230019 to D. Cherniak, and EAR-0106738 to F. Spear.

## REFERENCES CITED

Abraham, M.M., Boatner, L.A., Quinby, T.C., Thomas, D.K., and Rappaz, M. (1980) Preparation and compaction of synthetic monazite powders. Radioactive Waste Management, 1, 181–191.

Anthony, J.W. (1957) Hydrothermal synthesis of monazite. American Mineralogist, 42, 904.

——— (1965) Crystal morphology of thorium-bearing synthetic monazite. American Mineralogist, 50, 1421–1431.

Ball, D. and Wanklyn, B.M. (1976) Coloured synthetic zircon crystals: Flux growth and EPR of $V^{4+}$ impurity ions. Physica Status Solidi B, 36, 307–316.

Ballman, A.A. and Laudise, R.A. (1965) Crystallization and solubility of zircon and phenacite in certain molten salts. Journal of the American Ceramic Society, 48, 130–133.

Boatner, L.A. and Sales, B.C. (1988) Monazite. In W. Lutze and R.C. Ewing, Eds., Radioactive Waste Forms for the Future, p. 495–564. Elsevier, North-Holland, Amsterdam.

Bondar, I.A., Domanskii, A.I., Mezentseva, L.P., Degen, M.G., and Kalinia, N.E. (1976) Physiochemistry of rare-earth orthophosphates. Journal of Inorganic Chemistry, 21, 1126.

Bruker AXS Inc. (2001) Smart. Bruker AXS Inc., Madison, Wisconsin, U.S.A.

Chase, A.B. and Osmer, J.A. (1966) Growth and preferential doping of zircon and thorite. Journal of the Electrochemical Society, 113, 198–199.

Cherniak, D.J., Watson, E.B., Grove, M., and Harrison, T.M. (2004) Pb diffusion in monazite: A combined RBS/SIMS study. Geochimica et Cosmochimica Acta, 68, 829–840.

Ehrenhaut, D. and Pollnau, M. (2002) Flux growth of baryte-type $BaSO_4$ from chloridic alkaline metal solvents. Journal of Crystal Growth, 234, 533–538.

Espig, H. (1960) Synthesis of emerald. Chemistry and Technology, 12, 327–331.

Feigelson, R.S. (1964) Synthesis and single-crystal growth of rare-earth orthophosphates. Journal of the American Ceramic Society, 47, 257–258.

Fujii, S., Sugie, Y., Kobune, M., and Yamamoto, T. (1992) Effects of $Li_2O$ and $Na_2O$ addition on growth and electrical properties of $PbTiO_3$ single crystals. Journal of the Ceramic Society of Japan, 100, 1179–1183.

Jercinovic, M.J. and Williams, M.L. (2004) Analytical perils (and progress) in electron microprobe trace element analysis applied to geochronology: background acquisition, interferences, and beam irradiation effects. American Mineralogist, in press.

Montel, J.-M. (1989) Monazite end-members and solid solutions: synthesis, unit-cell characteristics, and utilization as microprobe standards. Mineralogical Magazine, 53, 120–123.

Montel, J.-M., Devidal, J.-L., and Avignant, D. (2002) X-ray diffraction study of brabantite-monazite solid solutions. Chemical Geology, 191, 89–104.

Nekrasov, I.Y. and Novikov, M.P. (1991) Isomorphic substitution capacity of monazite for rare earth elements. Doklady Akademii Nauk SSSR, 320, 963–966.

Pyle, J.M. (2001) Distribution of select trace elements in pelitic metamorphic rocks: pressure, temperature, mineral assemblage, and reaction-history controls. Ph.D. thesis, Rensselaer Polytechnic Institute, 352 p.

Pyle, J.M., Spear, F.S., Rudnick, R.L., and McDonough, W.F. (2001) Monazite-xenotime-garnet equilibrium in metapelites and a new monazite-garnet thermometer. Journal of Petrology, 42, 2083–2107.

Pyle, J.M., Spear, F.S., Wark, D.A., Daniel, C.G., and Storm, L.C. (2004) Contributions to precision and accuracy of chemical ages of monazite. American Mineralogist, in press.

Rappaz, M., Boatner, L.A., and Abraham, M.M. (1980) EPR investigations of $Gd^{3+}$ in single crystals and powders of the zircon-structure orthophosphates $YPO_4$, $ScPO_4$, and $LuPO_4$ [radioactive waste containment materials]. Journal of Chemical Physics, 73, 1095–1103.

Rappaz, M., Abraham, M.M, Ramey, J.O., and Boatner, L.A. (1981) EPR spectroscopic characterization of $Gd^{3+}$ in the monazite-type rare-earth orthophosphates: $LaPO_4$, $CePO_4$, $PrPO_4$, $NdPO_4$, $SmPO_4$, and $EuPO_4$. Physical Review B (Condensed Matter), 23, 1012–30.

Samatov, M.V., Votyakov, S.L., and Krasnobaev, A.A. (1982) Paramagnetic impurity centers in single crystals of synthetic xenotime. Izvestiya Akademii Nauk SSSR, Neorganicheskie Materialy, 18, 1866–1868.

Scott, V.D., Love, G., and Reed, S.J.B. (1995) Quantitative Electron-Probe Microanalysis (second edition). Ellis Horwood, New York.

Smith, S.H. and Wanklyn, B.M. (1974) Flux growth of rare earth vanadates and phosphates [and some magnetic properties]. Journal of Crystal Growth, 21, 23–28.

Suzuki, K., Kouta, H., and Nagasawa, H.H. (1992) Hf-Zr interdiffusion in single crystal zircon. Geochemical Journal, 26, 99–104.

Wanklyn, B.M. (1977) The prediction of starting compositions for the flux growth of complex oxide crystals. Journal of Crystal Growth, 37, 334–342.

——— (1978) Effects of modifying starting compositions for flux growth. Journal of Crystal Growth, 43, 336–344.

——— (1983) The present status of flux growth. Journal of Crystal Growth, 65, 533–540.

Wanklyn, B.M., Garrard, B.J., and Smith, S.H. (1983) Supersaturation, supercooling and flux growth of rare-earth phosphates. Journal of Crystal Growth, 63, 77–82.

MANUSCRIPT RECEIVED JANUARY 6, 2004
MANUSCRIPT ACCEPTED MARCH 22, 2004
MANUSCRIPT HANDLED BY JOHN AYERS